MR. TAHER CHEGINI (Orcid ID : 0000-0002-5430-6000)
MR. GUSTAVO DE ALMEIDA COELHO (Orcid ID : 0000-0003-2887-1118)

Article type : Technical Paper

A Novel Framework for Parametric Analysis of Coastal Transition Zone Modeling

Taher Chegini, Gustavo de A. Coelho, John Ratcliff, Celso M. Ferreira, Kyle Mandli, Patrick Burke, and Hong-Yi Li

Civil and Environmental Engineering (Chegini, Li), University of Houston, USA; Sid and Reva Dewberry Department of Civil, Environmental and Infrastructure Engineering (Coelho, Ferreira), George Mason University, USA; UNC Institute of Marine Sciences (Ratcliff), University of North Carolina at Chapel Hill, USA; Columbia University (Mandli); National Ocean Atmospheric Administration, National Ocean Service, Center for Operational Oceanographic Products and Services (Burke); (Correspondence to Taher Chegini: tchegini@central.uh.edu).

RESEARCH IMPACT STATEMENT: Introduces a framework for large scale analyses of physical processes affecting coastal dynamics to assist in planning and management of coastal areas at local to regional scales.

ABSTRACT: Vulnerability of coastal regions to extreme events motivates an operational coupled inland-coastal modeling strategy focusing on the coastal transition zone (CTZ), an area between the coast and upland river. To tackle this challenge, we propose a top-down framework for investigating the contribution of different processes to the hydrodynamics of CTZs with various geometrical shapes, different physical properties, and under several forcing conditions. We further propose a novel method, called Tidal Vanishing Point (TVP), for delineating the

extent of CTZs through the upland. We demonstrate the applicability of our framework over the US East and Gulf coasts. We categorize CTZs in the region into three classes, namely, without estuary (direct river-coast connection), triangular-, and trapezoidal-shaped estuary. The results show that although semi-diurnal tidal constituents are dominant in most cases, diurnal tidal constituents become more prevalent in the river segment as the discharge increases. Also, decreasing the bed roughness value promotes more significant changes in the results than increasing it by the same value. Additionally, the estuary promotes tidal energy attenuation and consequently decreases the reach of tidal signals through the upland. The proposed framework is generic and extensible to any coastal region.

(**KEYWORDS:** rivers/streams, flooding, hydrodynamics, fluvial processes, tides, coastal transition zones)

INTRODUCTION

Development, operation, and management of infrastructure located in coastal areas require accurate estimations of water level ranges, magnitude, and frequencies in the areas between the coast and the upland where tides no longer influence water level variation, i.e., the coastal transition zone (CTZ) (Couasnon et al., 2020; Moritz et al., 2016). For this purpose, an initiative is underway to enhance the National Water Model (NWM) (NOAA, 2016) by including water level predictions in CTZs (Bakhtyar et al., 2020). However, coupling the NWM to existing coastal hydrodynamic models in operational settings presents challenges such as increasing computational complexity and a priori parameter estimations (e.g., Garzon & Ferreira, 2016). Understanding the processes that contribute to water levels in CTZs, such as mean sea level, tidal range, river discharge, and storm surge, is essential to tackling these challenges (e.g., Camus et al., 2021; Du et al., 2018; Ghanbari et al., 2021; Hsiao et al., 2021; Valle-Levinson et al., 2020). The combined effect of these components is called the total water level (TWL) and the contribution of each component may vary based on the location of a CTZ.

Numerous studies mathematically defined the relationships between frictional and topographical factors, and their respective and combined influence on the tidal amplification in estuaries (e.g., Jay, 1991; Jena et al., 2018; Lanzoni & Seminara, 1998). Some studies have also examined the effects of longitudinally cross-sectional convergence of estuaries on tidal signal propagation. Friedrichs & Aubrey (1994) and Jay (1991) show that convergence significantly influences amplitudes of tidal constituents and velocity fields. Additionally, Lanzoni & Seminara (1998) suggest that the rate of convergence and non-linear responses, such as the generation of

overtides, play a key role in the tidal signal propagation through the upland. Moreover, Talke & Jay (2020) demonstrate the influence and importance of tidal resonance on the amplification of water levels through mathematical analysis.

Many published works feature case studies that examine coastal models' sensitivities to input parameters in specific regions (e.g., Garzon & Ferreira, 2016; Sohrt et al., 2021). Akbar et al. (2017) examined the effects of variations in bottom friction on water levels during a landfalling hurricane in the Gulf of Mexico. Moreover, Alebregtse & de Swart (2016) use a semi-analytical model to study the effect of river discharge on the propagation of tidal waves in the Yangtze estuary, in China. They show that when increasing river discharge, the amplitude of semi-diurnal sea surface elevation decreases. Calero Quesada et al. (2019) study the Guardiana estuary, in Spain and demonstrate that river discharge could influence tidal propagation through estuaries. Harrison et al. (2021) investigate the sensitivity of two UK estuaries to high river discharge and sea-level rise scenarios. Additionally, some other site-specific studies, such as Khalid & Ferreira (2020), Maskell et al. (2014), and Valle-Levinson et al. (2020), demonstrate the significant role of geometric variations in inundation processes, particularly with the interaction between the river and storm surge.

However, Ward et al. (2020) and Harrison et al. (2021) argue that currently, many studies are site-specific, and they fall short in advancing our understanding of the dynamic seaward and landward extent of coastal interfaces across the scale. They suggest that researchers should instead steer their concerted effort toward multi-disciplinary regional-scale analysis of coastal interfaces. For example, Kerr et al. (2013) present a regional study in the Gulf of Mexico and show that due to energy dissipation at the seafloor, decreasing Manning's roughness results in increases in water levels and vice versa. Joyce et al. (2019) carry out a similar study in Puerto Rico and the U.S. Virgin Islands and based on the analysis of Hurricanes Irma and Maria conclude that the pressure deficit due to these hurricanes is the main driver in the water level response. Moreover, Du et al. (2018) perform numerical simulations on several idealized domains and nine realistic estuaries over the US East coast, to study the tidal responses to sea-level rise. They demonstrate a reduction in tidal range in narrow channels and large low-lying shallow areas under higher sea levels. Ghanbari et al. (2021) show that the northeast Atlantic and the western part of the Gulf coasts are the most exposed to compound flood hazards based on the assessment of 26 paired tidal-riverine stations on the US coast.

In an effort toward regional-scale analysis of coastal areas, we propose a top-down framework for investigating the contributions of different processes and parameters to TWL

prediction in CTZs. This framework takes into account the effects of geometrical shapes, physical properties, and forcing conditions. We achieve this goal in two steps: First, we decompose the complex coastal hydrodynamic system into simpler physical processes according to data analysis of a region of interest. Second, we study these processes individually to gain more insights into their role in coastal dynamics. We carry out such a study on each process through sensitivity analyses of their corresponding model parameters. For this purpose, we perform numerous numerical simulations on idealized domains while relying on a complex coastal model that can capture intricacies of processes that contribute to coastal hydrodynamics. Using idealized domains allows for modeling numerous scenarios and studying the role of contributing processes in isolation. Additionally, this framework provides a novel method called Tidal Vanishing Point (TVP) for delineating the extent of a CTZ through the upland. This extent influences decisions on data exchange locations between an inland and a coastal model (i.e., hand-off location), which is an important consideration when optimizing the balance between accuracy and performance. Furthermore, insights into the respective significance of various physical parameters assist coastal modelers in model calibration and achieving computational efficiency by improving estimations of only relevant inputs or features.

This study demonstrates the applicability of the proposed framework by employing it for CTZs across the Gulf of Mexico and the US East Coast, where most of the US coastal areas with socio-economic importance are located. The structure of the rest of this paper is as follows. First, the methodology section describes the details of our proposed framework. Then, the results and discussion section present the statistical analyses on the spatially distributed model results for water surface heights and velocity fields, as well as the TVP estimations. The last section provides concluding remarks.

METHODOLOGY

This section describes details of our proposed framework for classifying CTZs and evaluating processes and parameters that influence TWL prediction. FIGURE 1 depicts a conceptual flowchart of the framework which we categorize into three groups: data analysis, modeling, and assessment.

[INSERT FIGURE 1 HERE]

Data analysis

The data analysis tasks deal with obtaining ground-truth and remote sensing data from various sources and extracting spatiotemporal summaries that provide insights into hydrodynamic characteristics of a region of interest. We determine these characteristics to parameterize the physical properties and forcing conditions in the region of interest.

Modeling

Upon obtaining summaries of physical properties and forcing conditions in a region of interest, we carry out a series of hydrodynamic simulations on idealized domains with simple geometries. For this purpose, we define a control model (a reference scenario) with some predetermined values for all the model parameters and then systematically perturb the parameters so we can study their contributions to the changes in the model behavior in isolation.

Assessment

We design the tasks in this category for gaining insights into the relative significance of contributing processes in coastal dynamics. For this purpose, we use the significance test concept for quantifying changes in some variables of interest caused by their perturbations. Additionally, we define a new concept called tidal vanishing point (TVP) for characterizing the reach of tidal signals through the upland, i.e., the extent of CTZs. The overall goal of the framework is to provide a mathematically rigorous and extensible blueprint for conducting sensitivity analyses on a set of model parameters that characterize the hydrodynamics of CTZs. We note that our proposed framework focuses on the relative significance of the parameters rather than absolute values.

Comparison Metrics (Significance Test). First, we assess the changes between each prediction and the reference scenario for a variable of interest through an error estimation metric such as mean absolute error (MAE) or root-mean-square error to obtain E_1 for the first prediction and E_2 for the second prediction. Then, we compute the mean and standard deviation of the obtained errors. Next, we determine the half-width of the confidence interval at a specified level on the difference between the mean errors ($\Delta E = E_2 - E_1$). We compute this half-width confidence interval using $CI_\alpha = \sqrt{2(1-\rho)} \times z^* \frac{\sigma}{\sqrt{n}}$ where ρ is the correlation coefficient (Pearson R) between the scores, σ is the standard deviation, α is the confidence level, z^* is the z -score value corresponding to α (e.g., it is 1.96 for 95% confidence interval), and n is the number of observation points. Finally, we compute $SD = \text{sign}(\Delta E) \times (\text{abs}(\Delta E) - CI_\alpha)$, which

measures the relative significance of the predictions' deviation from the reference scenario. A positive value means that the total change in scenario 2 is more significant than the total change in scenario 1 and vice versa for a negative value.

Tidal Vanishing Point. To determine the extent of CTZs influence through the upland, we devise a procedure based on fluctuations of the tidal constituents' amplitudes across the centerline of the domain. This method relies on the amplitudes of the tidal constituents from the water level time series at grid points along the domain's centerline that extends from the ocean boundary to the river discharge boundary. The computation procedure is as follows:

1. Determine the dominant tidal constituent(s) within each tidal constituent category based on their amplitudes: Semi-diurnal, diurnal, short period, and long period.
2. Determine the (signal) filtering window size based on a percentage of the centerline length. This percentage is a parameter that we can determine via trial-and-error.
3. Carry out three subsequent passes of low-pass filtering on the amplitudes.
4. Compute exceedance probability for the filtered amplitudes.
5. Determine a threshold for amplitudes of each constituent, below which we consider the fluctuations negligible. We determine this threshold with trial-and-error based on a percentage of the exceedance probability.
6. Compute locations across the centerline where the amplitudes onward fall below the thresholds for each constituent. We coin these locations Tidal Vanishing Points (TVPs). In some cases, we might not reach a TVP due to not long enough river length.
7. Aggregate the obtained TVPs by finding their maximum value for each constituent.

We elucidate all these steps through their application in a case study in the following section. Moreover, we note that extending the TVP concept from idealized domains to real coastal domains can be challenging due to its reliance on the trial-and-error method and the simplifications. Therefore, since this study applies this method to a subset of coastal areas, the extent of applicability of TVP for determining the reach of CTZs requires further analyses.

CASE STUDY

In this section, we demonstrate the details of our framework through its application across the US East and Gulf coasts.

Data Analysis

Retrieve Ground-truth and Remote Sensing Data. At the first step, we retrieve the required datasets in our study region (TABLE 1) and conduct a series of statistical analyses on them to obtain sensible ranges for the parameters that we need to support the model generation and define boundary conditions for simulation scenarios.

[INSERT TABLE 1 HERE]

According to the obtained water level observations, tides vary significantly over the study region, wherein amplitudes are smaller in the Gulf Coast than the East Coast. We evaluate the water level data from all monitoring stations in the study region under the tidal influence to determine the spatial distribution of the strongest tidal constituents in the region. As shown in FIGURE 2 a, based on data from the period 2000-2015, the M2 (principal lunar semi-diurnal) tidal constituent is the strongest over the East and most of Florida coast, while the K1 (a lunar diurnal constituent) is often the strongest tidal constituent in the Gulf. FIGURE 2 b-c show the seasonal variation of the mean range tide (MN) of the two strongest constituents (M2 and K1) where the mean tide range of K1-dominant stations has higher seasonal variability when compared with the M2-dominant stations. The mean tide range is the difference in height between mean high water and mean low water (NOAA, 2020). Although there are two types of dominant tides in the region, we only consider an M2-dominant tide in this study.

[INSERT FIGURE 2 HERE]

For determining limits of river discharge in the region, we use HyRiver (Chegini et al., 2021) Python package to collect mean daily discharge data from USGS monitoring stations located in streams where the processes in estuaries influence the flow (FIGURE 3 a). The USGS classifies the interaction between the stream and ocean waters into tide stream (ST-TS) and estuary (ES). An ST-TS station is located where the streamflow is influenced by the tide, but the water chemistry is not normally influenced. An ES station is located at the coastal inlet of the ocean where the water normally mixes with stream water (USGS, 2021). Out of 390 ST-TS and ES stations, 26 have mean daily discharge data that we use for computing a summary of discharges in our study region (FIGURE 3 b). We consider the mean of means (eq. 1) as the lower limit and the mean of peaks (eq. 2) as the upper limit for the river discharge values at the upstream boundary. We compute these two mean values using:

$$\mu_{\bar{x}} = \frac{\Sigma \bar{x}_i}{n} \tag{1}$$

$$\mu_{y} = \frac{\Sigma y_i}{n} \tag{2}$$

where $\mu_{\bar{x}}$ is mean of means, $\bar{x}_i$ is mean discharge for station i, μ_y is mean of peaks, y_i is peak discharge for station i, and n is the total number of stations.

[INSERT FIGURE 3 HERE]

At the next step, we determine the range of peak storm surge heights based on a statistical analysis of extreme water level data over the study region and in the period 2000-2015. The extreme water levels (FIGURE 4 a) are 1% exceedance probability of water levels above mean higher high water (MHHW). MHHW is the tidal elevation determined by averaging the higher of each day's two high tides at a particular location over a recorded history (NOAA, 2020). We consider the minimum (0.769 m) and the maximum (3.154 m) values of the data as the lower and higher limits for the peak storm surge height, respectively.

[INSERT FIGURE 4 HERE]

The bed slope is another important physical property that influences coastal dynamics. We obtain the limits of this parameter in the Gulf and East coasts from Hammar-Klose & Thieler (2001). FIGURE 4 b presents the coastal slope map of the region, where the slope varies from zero in the Gulf region to over 0.4% in the upper regions of the East coast.

Classification of CTZs. We define a series of idealized domains based on a classification of river-estuary systems (RESs) in the study region. For this purpose, we retrieve over 400 black and white satellite images of the RESs from the Stamen (2019) map service. We opt for black and white images to facilitate their visual inspection in the next step i.e., manual labeling. We sift through the images and delineate the smallest enclosing polygon for each RES (FIGURE 5 a-c).

[INSERT FIGURE 5 HERE]

The manual labeling of RESs in the region suggests that either there is no estuary (direct river-coast connection), or the estuaries are mainly triangular- or trapezoidal-shape. For parameterizing these geometries, we further narrow down the obtained RES images to 46 cases where sizes of their geometric shapes are representative of the whole collection (FIGURE 6). We introduce three ratios to establish relationships among them, as follows:

$$R_{lb} = \frac{L_b}{W_b} \quad (1)$$

$$R_{bt} = \frac{W_b}{W_t} \quad (2)$$

$$R_{br} = \frac{W_b}{W_r} \quad (3)$$

where L_b is the estuary length, W_b is the downstream estuary width, W_t is the upstream estuary width (for trapezoidal estuaries), and W_r is the river width (FIGURE 7 a). We should note that

our parameterization and delineation strategies are specific to the region of our study and are not a general classification of coastal areas. Thus, applying this framework to other regions will probably require modifications to the shapes and their parameters.

[INSERT FIGURE 6 HERE]

[INSERT FIGURE 7 HERE]

Based on a statistical analysis of the 46 RESs, the mean and median of R_{br} are 10.1 and 8.1 respectively, with higher values appearing above a latitude of 37°. Moreover, the median of R_{lb} is 2.2 and triangular shapes usually have higher values and are between latitudes 32° and 38° (TABLE 2).

[INSERT TABLE 2 HERE]

Consequently, we categorize the CTZs into three classes, namely, without estuary (direct river-coast connection) (C1), triangular-shaped estuary (C2), and trapezoidal-shaped estuary (C3). Additionally, to account for other geometric elements with significant effects in hydrodynamic modeling of RESs, we introduce three categories within each class: a straight-line river (A), a sinuous river (B), and an estuary with island barriers (C) (FIGURE 7 b).

Modeling using idealized domains

Mesh and Physical Properties. We generate an idealized domain for each category and class (FIGURE 7 b), each of which has two or three segments (ocean, estuary, and river) according to their respective classes.

We consider category 1 models as the reference model when investigating multiple categories. We set the length of the ocean segment to100 km (perpendicular to the coast) and its width to 50 km width (parallel to the coast) for ensuring that boundaries do not affect the region of interests (FIGURE 8 a). Then, we generate the ocean mesh with approximately 17K nodes with varying grid resolution between 250 m and 1 km. Based on the mean of R_{br} values, we set the length of the river segment for the reference model (category 1) to 1,000 km, and its width (W_r) to 1 km. The grid spacing of the river mesh is 250-m in the width direction and 1-km along the river (approximately 5K nodes). Considering the geometric shapes in our study, we adopt the downstream width of the estuary (W_b) as the independent parameter for scaling the idealized models. For all configurations with estuaries (classes 2 and 3), we set W_b to 10 km, based on the sampling mean and median of the data (TABLE 2). Moreover, the estuary length (L_b) for the reference case is 20 km which is the median value of R_{lb}. The estuary mesh resolution varies between 250 m and 1 km, providing a smooth transition between the ocean and the river

(approximately 2K nodes). FIGURE 8 b depicts an example of such a mesh that we generated for the model C2A.

[INSERT FIGURE 8 HERE]

The bathymetry is variable parallel to the river direction and constant along the perpendicular to the river direction. FIGURE 8 shows the bottom elevation of the domain. Based on the collected coastal slope data (FIGURE 4 d), we use 0.055% for the bed slope of the ocean segment for all the models. At the river mouth, we choose a value for the depth larger than the maximum tidal amplitude to minimize the influence of the bottom in the tidal wave propagation and avoid the wave amplification as a result of bottom-wave interaction. Also in the river segment, we set the bottom elevation at the upstream boundary to -1 m, allowing the water to propagate upstream, and enabling the estimation of the TVP and delineation of the CTZ.

For category B, we consider a river sinuosity of 1.45. The sinuosity is the ratio of channel length over valley length. For category C, we set the opening of the barriers that enclose the mouth of the estuary to 2 km, equivalent to 20% of the estuary width. While categories B and C were also implemented and studied, for brevity, in the result section we only present the results of Category A (straight river) for the three classes.

We conduct the simulations using the hydrodynamic model, D-Flow Flexible Mesh (D-Flow FM) of the Delft3D Flexible Mesh Suite developed by Deltares (2019), with unstructured grids configured to perform 2D simulations. Although we use idealized domains to demonstrate this framework, the D-Flow FM solves the Navier-Stokes equations for an incompressible fluid, under the shallow water and the Boussinesq assumptions (Deltares, 2019), which can represent complex non-linear processes such as tidal propagation, backwater effect, and turbulence.

Boundary Conditions and Scenarios. We select a set of scenarios to perform the simulations and boundary conditions using ground-truth and remote sensing data. Based on the reference scenarios, we establish a procedure for setting up simulation by only changing one parameter per scenario, allowing the quantification of the contribution of the input parameters to the output results. We define these simulation scenarios based on uniform Manning's roughness at the bed level (R), the upstream river discharge (D), and the water level at the ocean boundary (T). We use two types of water level time series at the ocean boundary; predicted tides (P) and storm surge that superimposes a surge pulse onto the predicted tides (S) (TABLE 3).

[INSERT TABLE 3 HERE]

We select a location for obtaining water level data based on proximity to a station from the National Oceanic and Atmospheric Administration (NOAA) National Water Level

Observation Network (NWLON) with a considerable number of samples of higher tide amplitude during an extreme event. In this study, we opt for the NOAA station at Atlantic City, NJ (Lat = 39°21.4' N, Lon = -74°25.1', ID = 8534720) where Hurricane Sandy made landfall (22-29 Oct 2012). Subsequently, we use the water level predictions by NOAA's Operational Oceanographic Products and Services (CO-OPS) at this station during the period between 10 Oct – 10 Nov 2012 as the baseline water level boundary condition at the ocean boundary (FIGURE 9) for all scenarios. Following the approach presented in Perrin et al. (2021) for storm surge analysis, we superimpose an isosceles triangular surge pulse on the baseline water level time series. However, instead of their parametrization approach, we consider the surge peak height (amplitude) as the only surge parameter and use a constant duration of two days for the rising and falling limbs of the pulse. Then, we produce two storm surge scenarios, S07 and S31, based on the minimum (0.769 m) and maximum (3.154 m) values of extreme water levels (above MHHW) that we obtained over the Gulf and US East coast during 2000-2015 period.

[INSERT FIGURE 9 HERE]

For the reference scenario, we set the discharge at the upstream boundary to 0 m^3/s. Then, we define two discharge scenarios (D) based on the mean of means (90 m^3/s) and mean of peaks (570 m^3/s) values that we obtain from the analysis of discharge data from USGS stations under the tidal influence (FIGURE 3). We use 30 days as the simulation duration for the scenarios (10 Oct – 10 Nov 2012) with a warm-up period of 5 days, i.e., the analyses of the results are based on 25 days (15 Oct – 10 Nov 2012).

Assessment of water surface height and velocity field

Significance Test. In this study, we opt for using the Mean Absolute Error (MAE) as a metric for measuring the total change between a scenario and the reference scenario. The significance test quantifies the relative significance of changes in a variable of interest between two competing predictions to a reference scenario (Jolliffe & Ebert, 2017). We consider the water surface height and velocity field as the variables of interest and adopt 95% as the confidence level.

Tidal Vanishing Point. In the study case, we take into account three of the four tidal constituents' categories, namely semi-diurnal, diurnal, and short period (overtides). As the simulation period in our study is one month, we do not include the long-period tidal constituents. For determining the dominant tidal constituent(s) in each category, we compare fluctuations of their amplitudes across the domain. Additionally, with trial-and-error, we determine the filtering

window width of 2% of the centerline length and adopt 50% exceedance probability as the threshold to estimate TVPs for each scenario.

RESULTS AND DISCUSSION

In this section, we present the results obtained from the application of our proposed framework to the US Gulf and East coast. While not attempting to provide a comprehensive analysis of all parameters contributing to TWL predictions, this section details the required steps for effective implementation of the framework and elucidates interpreting the outputs for gaining insights into the interplay of the parameters.

Significance Test

FIGURE 10 and FIGURE 11 show the spatial distribution of the MAE Significance Test for water surface height and velocity field, respectively. The rows correspond to the parameters, i.e., discharge (D), bed roughness (R), and storm surge (S), while columns are the classes, i.e., without estuary (C1), triangular-shaped estuary (C2), and trapezoidal-shaped estuary (C3). For a specific parameter and class, the values in the color bar on the right indicate the relative significance of the changes in the corresponding scenarios.

Discharge. The significant difference in the discharge scenarios is shown in FIGURE 10 a-c, where greater differences are observed above approximately 300 km through the upland (y-axis) and are more pronounced in the higher discharge scenario (D570). In the lower river reach and estuary, there is no significant difference between both discharge scenarios. When there is no estuary (FIGURE 10 a), there is a significant difference in water surface heights along the longer part of the river section in comparison to the other classes (FIGURE 10 b-c). This difference suggests that the estuary area attenuates the tidal energy coming from the ocean. However, as we approach the mouth of the river, the discharge has a stronger influence on water level (FIGURE 10 b-c) and velocity field (FIGURE 11 b-c) in the cases with an estuary. Additionally, we note the stronger influence of discharge in the river segment in class 3 (FIGURE 10 c and FIGURE 11 c), where the sharper edges of the trapezoidal-shaped estuary increase the dissipation of the tidal energy that enters the domain from the ocean boundary. Calero Quesada et al. (2019) reports a similar finding in their study of Guardiana estuary, in Spain. Harrison et al. (2021) also found that the impact of higher discharges is more relevant in upper and smaller estuaries while investigating two estuaries in the UK.

Roughness. In the bed roughness scenarios, since there is no river discharge in the upstream boundary, the tide from the ocean boundary is the only force in the domain. The reduction of Manning's roughness in scenario R20 results in a significant difference in comparison to the R30 scenario (FIGURE 10 d-f and FIGURE 11 d-f) which corroborates the findings of Akbar et al. (2017) in their study on Hurricane Rita. Also, there is a greater difference in water level in class 2 along the river.

Some studies (e.g., Savenije & Veling, 2005; Van Rijn, 2011) have shown that the balance between the rate of convergence of the channel and the bed friction influences the magnitude of wave propagation dampening through a channel. This additional convergence effect near the mouth of the river due to the triangular shape of the C2 class appears to shift this balance, thereby creating more significant differences due to changes in bed roughness values.

The significance of differences in the velocity field is stronger and goes farther upstream of the river when there is no estuary (FIGURE 11 d). These results suggest that the estuary promotes tidal energy attenuation and reduces the impact of the bed roughness changes along the river. Moreover, due to the higher dissipation of energy in the trapezoidal estuary due to the sharp edges, the greatest changes in the velocity field occur near the estuary, but they are weaker through the upland (FIGURE 11 f).

Storm Surge. In this scenario analysis, we notice significant differences both in water level (FIGURE 10 g-i) and velocity field (FIGURE 11 g-i) for the higher storm surge peak (S31) scenario. Moreover, in both cases, the storm surge leads to more prominent changes through the river in the without estuary case and these changes propagated farther through the upland (FIGURE 10 g). Again, we see the attenuating role of the estuaries in these simulations, where a decrease in the significance values is observed when going upstream of the river (FIGURE 10 h-i). We notice no significant difference in the results for classes 2 (FIGURE 10 h and FIGURE 11 h) and 3 (FIGURE 10 i and FIGURE 11 i).

[INSERT FIGURE 10 HERE]

[INSERT FIGURE 11 HERE]

Tidal Vanishing Point

In the analysis of the tidal vanishing point, we apply the proposed framework considering three tidal constituents' categories: semi-diurnal (e.g., M2, S2), diurnal (e.g., K1, O1), and overtides or shallow-water tides (e.g., M4, M6) since the long period category is not applicable (simulation period is one month). First, we decompose the water level time series for each grid

point along the centerline of the domain into its tidal constituents using the Python implementation of the UTide package (Codiga, 2011). Then we identify the strongest tidal constituent of each category based on the obtained amplitudes. For example, FIGURE 12 shows a comparison of the constituents in each category for the C1 D570 scenario (without estuary and with river discharge of 570 m^3/s). The results suggest that in the semi-diurnal category, M2 is dominant; in the diurnal category, both O1 and K1 are dominant; and in the overtide category, M4 is the dominant constituent.

[INSERT FIGURE 12 HERE]

Subsequently, we compute the rolling window average using a window width of 2% of the centerline length. We use a threshold value of the amplitude corresponding to the 50% exceedance probability for determining the TVPs. FIGURE 13 shows the effect of using different threshold values on the TVP estimation.

[INSERT FIGURE 13 HERE]

We carry out the significance test strategy based on the obtained values for the window width and the threshold. The results suggest that M2 is the dominant tidal constituent mainly in the ocean segment of the domain, while in the river segment K1 and O1 are stronger, especially when the river discharge is high. Moreover, M4 is the dominant overtide, with stronger influence near the estuary. FIGURE 14 shows the results of the tidal amplitude and TVP for the strongest tidal constituents (i.e., M2, K1, O1, and M4) in the selected categories, and TABLE 4 presents a summary of the obtained TVP locations.

Semidiurnal tidal constituent. We notice a lower decay rate of the amplitude for the M2 tidal constituent for class 1 (FIGURE 14 a) in comparison to classes 2 (FIGURE 14 b) and 3 (FIGURE 14 c), demonstrating the attenuation of the tidal propagation by the estuaries. In storm surge scenario S31, the tidal signal propagates farther upstream when compared with scenario S07 which has a lower surge peak. The TVP for the discharge scenario D570 does not show significant changes across the three classes.

Diurnal tidal constituents. The results for these constituents show higher amplitudes for scenarios S31 and D570 along the river reach (FIGURE 14 d-i). The K1 and O1 constituents are dominant, even stronger than semi-diurnal constituents upstream of the river. Moreover, in the D570 case (FIGURE 14 d-i) the TVP occurs outside the domain, i.e., the river is not long enough, so the two competing forces (tide from the ocean boundary and discharge from the river boundary) can reach an equilibrium.

Shallow-water tides. The results suggest that the TVPs are closer to the shore when increasing the bed roughness, i.e., R30 vs. R20 (FIGURE 14 j-k). On the other hand, the results for the two surge scenarios show that the TVP in scenario S07 is closer to the ocean than for scenario S31 (FIGURE 14 j-l).

[INSERT FIGURE 14 HERE]

CONCLUSIONS

The objective of this study is to devise a top-down framework for investigating and conducting quantitative analysis of different processes and parameters that contribute to coastal hydrodynamics. We achieve this goal by parameterizing the physical processes that contribute to the complex coastal hydrodynamic behavior through analyses of ground-truth and remote sensing data in a region of interest and performing numerous simulations to study the significance of each process in isolation. The main findings are listed below:

1) We present a method to classify and parameterize CTZs that facilitates the correlation of the results found in the idealized models to real-world scenarios. We demonstrate this method by introducing one independent and three dependent variables for generating idealized CTZ domains based on the analysis of over 400 RESs along the US East and Gulf coasts. Further investigations based on unexplored geometries and ratios would help to expand the applicability of the results to real-world scenarios.
2) The analysis of discharge demonstrates that although semi-diurnal tidal constituents are dominant in most cases, as the discharge increases, diurnal tidal constituents become more dominant in the river segment. Therefore, the reach of tidal signals can extend farther through the upland as the discharge increases. Also, the analysis of bed roughness suggests that decreasing it promotes more significant changes in the results than increasing it by the same value. Moreover, the analysis of storm surge shows that the estuary promotes tidal energy attenuation and consequently decreases the reach of tidal signals through the upland.
3) We propose a novel method for delineating the reach of tidal signals through the upland called Tidal Vanishing Point based on the amplitude of dominant tidal constituents. This method can assist coastal and hydrological modelers with deciding on the hand-off region between a computationally cheap inland model and a computationally expensive coastal model.

Although this study does not provide a comprehensive study of all parameters and complexities associated with the CTZs, the proposed framework is generic and extensible. It

provides a systematic approach for determining the most significant processes and parameters influencing TWL predictions. The procedure could be applied to different coastal areas that would assist modelers during the processes of preparing, running, and analyzing coastal models.

ACKNOWLEDGMENTS

We are thankful to the Editor and anonymous reviewers for their comments and suggestions, which helped to improve the quality of the manuscript. This research was produced as part of the 2019 National Water Center Summer Institute, which was supported by funding from the National Science Foundation to the Consortium of Universities for the Advancement of Hydrologic Science, Inc. (CUAHSI). T. Chegini was also supported by the University of Houston's internal funds. H.-Y. Li was supported by the U.S. Department of Energy's Office of Science, as part of the Earth System Model Development, Earth and Environmental System Modeling Program.

DATA AVAILABILITY STATEMENT

The data that support the findings of this study are openly available in GitHub at https://github.com/cheginit/coastal_transition_zone

LITERATURE CITED

Akbar, M. K., Kanjanda, S., & Musinguzi, A. (2017). Effect of bottom friction, wind drag coefficient, and meteorological forcing in hindcast of Hurricane Rita storm surge using SWAN + ADCIRC model. *Journal of Marine Science and Engineering*, *5*(3), 38. https://doi.org/10.3390/jmse5030038

Alebregtse, N. C., & de Swart, H. E. (2016). Effect of river discharge and geometry on tides and net water transport in an estuarine network, an idealized model applied to the Yangtze Estuary. *Continental Shelf Research*, *123*, 29–49. https://doi.org/10.1016/j.csr.2016.03.028

Bakhtyar, R., Maitaria, K., Velissariou, P., Trimble, B., Mashriqui, H., Moghimi, S., Abdolali, A., Van der Westhuysen, A. J., Ma, Z., Clark, E. P., & Flowers, T. (2020). A New 1D/2D Coupled Modeling Approach for a Riverine-Estuarine System Under Storm Events: Application to Delaware River Basin. *Journal of Geophysical Research: Oceans*, *125*(9). https://doi.org/10.1029/2019JC015822

Calero Quesada, M. C., García-Lafuente, J., Garel, E., Delgado Cabello, J., Martins, F., & Moreno-Navas, J. (2019). Effects of tidal and river discharge forcings on tidal propagation

along the Guadiana Estuary. *Journal of Sea Research*, *146*, 1–13. https://doi.org/10.1016/j.seares.2019.01.006

Camus, P., Haigh, I. D., Nasr, A. A., Wahl, T., Darby, S. E., & Nicholls, R. J. (2021). Regional analysis of multivariate compound coastal flooding potential around Europe and environs: Sensitivity analysis and spatial patterns. *Natural Hazards and Earth System Sciences*, *21*(7), 2021–2040. https://doi.org/10.5194/nhess-21-2021-2021

Chegini, T., Li, H.-Y., & Leung, L. R. (2021). HyRiver: Hydroclimate Data Retriever. *Journal of Open Source Software*, *6*(60), 3175. https://doi.org/doi.org/10.21105/joss.03175

Codiga, D. L. (2011). *Unified Tidal Analysis and Prediction Using the UTide Matlab Functions. Technical Report 2011-01.* ftp://www.po.gso.uri.edu/pub/downloads/codiga/pubs/%0A2011Codiga-UTide-Report.pdf

Couasnon, A., Eilander, D., Muis, S., Veldkamp, T. I. E., Haigh, I. D., Wahl, T., Winsemius, H. C., & Ward, P. J. (2020). Measuring compound flood potential from river discharge and storm surge extremes at the global scale. *Natural Hazards and Earth System Sciences*, *20*(2), 489–504. https://doi.org/10.5194/NHESS-20-489-2020

Deltares. (2019). *Delft3D flexible Mesh suite 1D/2D/3D Modelling suite for integral water solutions User Manual D-Flow Flexible Mesh*.

Du, J., Shen, J., Zhang, Y. J., Ye, F., Liu, Z., Wang, Z., Wang, Y. P., Yu, X., Sisson, M., & Wang, H. V. (2018). Tidal Response to Sea-Level Rise in Different Types of Estuaries: The Importance of Length, Bathymetry, and Geometry. *Geophysical Research Letters*, *45*(1), 227–235. https://doi.org/10.1002/2017GL075963

Friedrichs, C. T., & Aubrey, D. G. (1994). Tidal propagation in strongly convergent channels. *Journal of Geophysical Research*, *99*(C2), 3321. https://doi.org/10.1029/93JC03219

Garzon, J. L., & Ferreira, C. M. (2016). Marine Science and Engineering Storm Surge Modeling in Large Estuaries: Sensitivity Analyses to Parameters and Physical Processes in the Chesapeake Bay. *Journal of Marine Science and Engineering*, *4*(45). https://doi.org/10.3390/jmse4030045

Ghanbari, M., Arabi, M., Kao, S.-C., Obeysekera, J., & Sweet, W. (2021). Climate Change and Changes in Compound Coastal-Riverine Flooding Hazard Along the U.S. Coasts. *Earth's Future*, *9*(5), e2021EF002055. https://doi.org/10.1029/2021EF002055

Hammar-Klose, E. S., & Thieler, E. R. (2001). Coastal vulnerability to sea-level rise: a preliminary database for the U.S. Atlantic, Pacific, and Gulf of Mexico coasts. In *Data Series*. https://doi.org/10.3133/DS68

Harrison, L. M., Coulthard, T. J., Robins, P. E., & Lewis, M. J. (2021). Sensitivity of Estuaries to Compound Flooding. *Estuaries and Coasts*, *1*, 1–20. https://doi.org/10.1007/s12237-021-00996-1

Hsiao, S. C., Chiang, W. S., Jang, J. H., Wu, H. L., Lu, W. S., Chen, W. B., & Wu, Y. T. (2021). Flood risk influenced by the compound effect of storm surge and rainfall under climate change for low-lying coastal areas. *Science of the Total Environment*, *764*, 144439. https://doi.org/10.1016/j.scitotenv.2020.144439

Jay, D. A. (1991). Green's law revisited: Tidal long-wave propagation in channels with strong topography. *Journal of Geophysical Research*, *96*(C11), 20585. https://doi.org/10.1029/91JC01633

Jena, B. K., Sivakholundu, K. M., & Rajkumar, J. (2018). A description of tidal propagation in Hooghly estuary using numerical and analytical solutions. *Ocean Engineering*, *169*, 38–48. https://doi.org/10.1016/j.oceaneng.2018.09.009

Jolliffe, I., & Ebert, B. (2017). *How do I know whether one forecast system performs significantly better than another?* https://www.cawcr.gov.au/projects/verification/CIdiff/FAQ-CIdiff.html

Joyce, B. R., Gonzalez-Lopez, J., Van der Westhuysen, A. J., Yang, D., Pringle, W. J., Westerink, J. J., & Cox, A. T. (2019). U.S. IOOS Coastal and Ocean Modeling Testbed: Hurricane-Induced Winds, Waves, and Surge for Deep Ocean, Reef-Fringed Islands in the Caribbean. *Journal of Geophysical Research: Oceans*, *124*(4), 2876–2907. https://doi.org/10.1029/2018JC014687

Kerr, P. C., Martyr, R. C., Donahue, A. S., Hope, M. E., Westerink, J. J., Luettich, R. A., Kennedy, A. B., Dietrich, J. C., Dawson, C., & Westerink, H. J. (2013). U.S. IOOS coastal and ocean modeling testbed: Evaluation of tide, wave, and hurricane surge response sensitivities to mesh resolution and friction in the Gulf of Mexico. *Journal of Geophysical Research: Oceans*, *118*(9), 4633–4661. https://doi.org/10.1002/jgrc.20305

Khalid, A., & Ferreira, C. M. (2020). Advancing real-time flood prediction in large estuaries: iFLOOD a fully coupled surge-wave automated web-based guidance system. *Environmental Modelling and Software*, *131*, 104748. https://doi.org/10.1016/j.envsoft.2020.104748

Lanzoni, S., & Seminara, G. (1998). On tide propagation in convergent estuaries. *Journal of Geophysical Research: Oceans*, *103*(C13), 30793–30812. https://doi.org/10.1029/1998JC900015

Maskell, J., Horsburgh, K., Lewis, M., & Bates, P. (2014). Investigating River–Surge Interaction

in Idealised Estuaries. *Journal of Coastal Research*, *294*(2), 248–259. https://doi.org/10.2112/JCOASTRES-D-12-00221.1

Moritz, H., White, K., & Gouldby, B. (2016). An updated USACE approach to the evaluation of coastal total water levels for present and future flood risk analysis. *E3S Web of Conferences*, *7*, 01012. https://doi.org/10.1051/e3sconf/20160701012

NOAA. (2016). *National Water Model: Improving NOAA's Water Prediction Services*. http://water.noaa.gov/documents/wrn-national-water-model.pdf

NOAA. (2020). *NOAA Tides & Currents. Products. Datums. About Tidal Datums.* https://tidesandcurrents.noaa.gov/datum_options.html

Perrin, T. V. E., Roustant, O., Rohmer, J., Alata, O., Naulin, J. P., Idier, D., Pedreros, R., Moncoulon, D., & Tinard, P. (2021). Functional principal component analysis for global sensitivity analysis of model with spatial output. *Reliability Engineering and System Safety*, *211*, 107522. https://doi.org/10.1016/j.ress.2021.107522

Savenije, H. H. G., & Veling, E. J. M. (2005). Relation between tidal damping and wave celerity in estuaries. *Journal of Geophysical Research C: Oceans*, *110*(4), 1–10. https://doi.org/10.1029/2004JC002278

Sohrt, V., Hein, S. S. V., Nehlsen, E., Strotmann, T., & Fröhle, P. (2021). Model based assessment of the reflection behavior of tidal waves at bathymetric changes in estuaries. *Water (Switzerland)*, *13*(4), 489. https://doi.org/10.3390/w13040489

Talke, S. A., & Jay, D. A. (2020). Changing Tides: The Role of Natural and Anthropogenic Factors. *Annual Review of Marine Science*, *12*(1), 121–151. https://doi.org/10.1146/annurev-marine-010419-010727

USGS. (2021). *USGS Site Type Codes (site_tp_cd)*. https://maps.waterdata.usgs.gov/mapper/help/sitetype.html

Valle-Levinson, A., Olabarrieta, M., & Heilman, L. (2020). Compound flooding in Houston-Galveston Bay during Hurricane Harvey. *Science of The Total Environment*, *747*, 141272. https://doi.org/10.1016/j.scitotenv.2020.141272

Van Rijn, L. C. (2011). Analytical and numerical analysis of tides and salinities in estuaries; Part I: Tidal wave propagation in convergent estuaries. *Ocean Dynamics*, *61*(11), 1719–1741. https://doi.org/10.1007/s10236-011-0453-0

Ward, N. D., Megonigal, J. P., Bond-Lamberty, B., Bailey, V. L., Butman, D., Canuel, E. A., Diefenderfer, H., Ganju, N. K., Goñi, M. A., Graham, E. B., Hopkinson, C. S., Khangaonkar, T., Langley, J. A., McDowell, N. G., Myers-Pigg, A. N., Neumann, R. B.,

Osburn, C. L., Price, R. M., Rowland, J., … Windham-Myers, L. (2020). Representing the function and sensitivity of coastal interfaces in Earth system models. In *Nature Communications* (Vol. 11, Issue 1). https://doi.org/10.1038/s41467-020-16236-2

TABLES

TABLE 1. Datasets for obtaining sensible ranges for model parameters.

Dataset	Source	Period
Water Level Observations	Oceanographic Products and Services (CO-OPS)	2000-2015
Extreme Water Levels	Oceanographic Products and Services (CO-OPS)	2000-2015
Mean Daily River Discharge	National Water Information System (NWIS)	2000-2015
Coastal Slope	(Hammar-Klose & Thieler, 2001)	-
Tidal Constituents	Oceanographic Products and Services (CO-OPS)	-
Satellite Images	Stamen (2019) and Google Earth Pro	-

TABLE 2. Summary statistics of the representative dimensions of the 46 satellite images of RESs.

Statistic	W_b	R_{bt}	R_{br}	R_{lb}
Mean	11.9 km	17.2	10.1	4.7
Standard deviation	11.3 km	23.2	14.	5.7
Minimum	0.4 km	0.23	0.75	0.67
Median	8.9 km	1.7	8.1	2.2
Maximum	49 km	79	90	25

TABLE 3. Configurations of simulation scenarios. The water level at the ocean boundary (T) uses a water level time series based on NOAA's predicted tides (P) and the same predicted tides with a storm surge pulse superimposed (S).

Scenario	Roughness (R)	Discharge (D) [m3/s]	Ocean Boundary (T)
Reference (Ref)	0.025	0	P
R20	0.020	0	P
R30	0.030	0	P
S07	0.025	0	S = 0.769 m
S31	0.025	0	S = 3.154 m
D90	0.025	90	P
D570	0.025	570	P

TABLE 4. Locations of the tidal vanishing points relative to the ocean boundary in km.

Scenario	C1	C2	C3
Ref	OD*	1123.5	OD
R20	OD	1123.5	1038.5
R30	OD	939.5	OD
S07	746.5	655.5	552.5
S31	OD	846.5	746.5
D570	1018.5	1123.5	OD
D90	981.5	797.5	1050.5

*OD: Outside the domain i.e., the river length was not long enough to allow the amplitudes to fall below the threshold.

FIGURES

FIGURE 1. Flowchart showing the framework for studying the contribution of parameters affecting TWL prediction.

FIGURE 2. a) Map showing the strongest tidal constituents at NOAA water level stations, and monthly mean water level (WL) variations (datum is Mean Sea Level) for b) K1 (n=19) and c) M2 (n=66) dominant stations.

FIGURE 3. a) Map showing the location of USGS stations under the tidal influence with (n=29) and without (n=361) available mean daily discharge data after 2000; b) Discharge data at the selected 29 stations for the period 2000-2015 (mean of means = 90 m3/s and mean of peaks = 570 m3/s).

FIGURE 4. Map showing a) extreme water levels with 1% exceedance probability above MHHW and b) coastal slope.

FIGURE 5. Examples of a) satellite images that were retrieved for classifying CTZs along the US East and Gulf coast, as well as manual labeling and shape delineation for b) triangular, and c) trapezoidal estuaries.

FIGURE 6. Map showing the spatial distribution of the selected 46 triangular- and trapezoidal-shaped RESs in the study region.

FIGURE 7. A depiction of geometry measurements and labels in the classification. Classes are C1 for without estuary, C2 for triangular-shaped estuary, and C3 for the trapezoidal-shaped estuary. Categories are A for the straight-line river, B for the sinuous river, and C for estuary with barriers.

FIGURE 8. The reference model configuration.

FIGURE 9. Water level time series for the ocean boundary condition based on NOAA's predicted tides and two surge pulses based on the 1% of exceedance probability above MHHW. We determine the peak values of 0.769 m and 3.154 m based on extreme water levels (above MHHW) that we obtained over the Gulf and US East coast during the 2000-2015 period.

FIGURE 10. MAE significance test results for the water surface heights. Each idealized domain class (1 – without estuary, 2: triangular estuary, and 3: trapezoidal estuary) is presented in one column, while the scenario comparison is shown in each row (D570vs. D90: discharge, R30 vs. R20: roughness, S31 vs. S07: storm surge).

FIGURE 11. MAE significance test results for the velocity field. Each idealized domain class (1 – without estuary, 2: triangular estuary, and 3: trapezoidal estuary) is presented in one column, while the scenario comparison is shown in each row (D570 vs. D90: discharge, R30 vs R20: roughness, S31 vs S07: storm surge).

FIGURE 12. Example of the tidal constituent's dominance verification by categories for C1 D570 scenario (w/0 estuary and with river discharge set to 570 m^3/s.

FIGURE 13. Example of the tidal vanishing point estimation for different exceedance probability levels.

FIGURE 14. Tidal amplitude and vanishing point for the strongest tidal constituents in the scenarios.

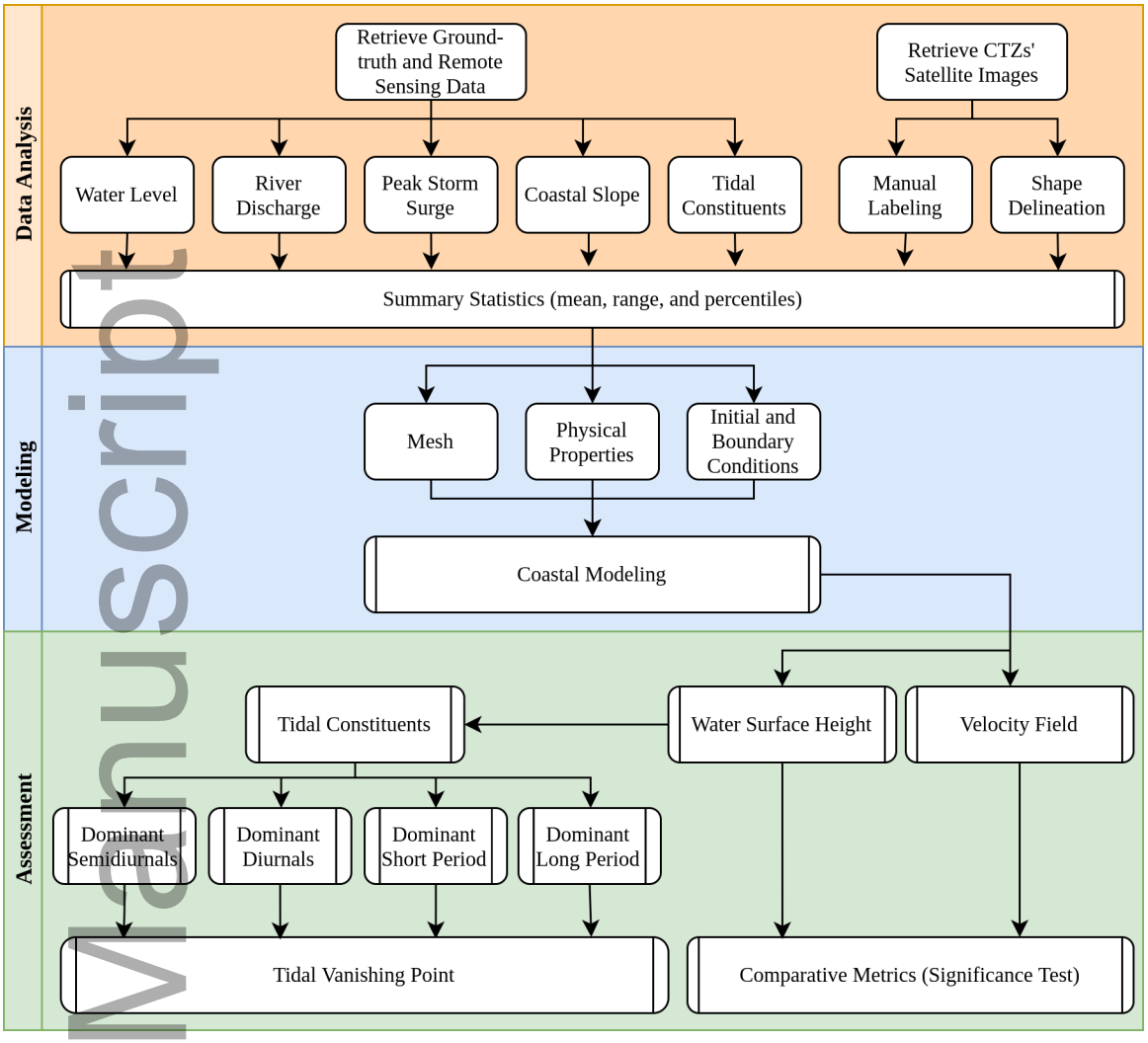

jawr_12983_f1.tiff

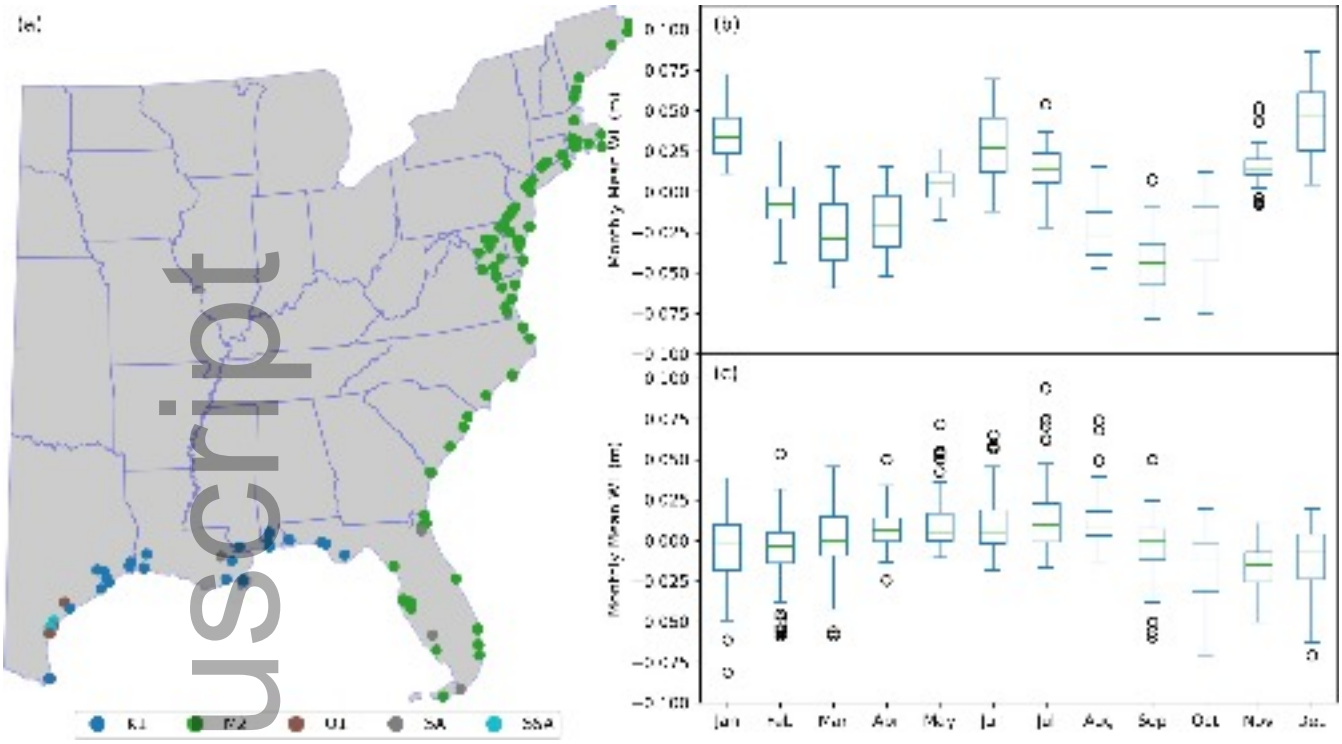

jawr_12983_f2.tiff

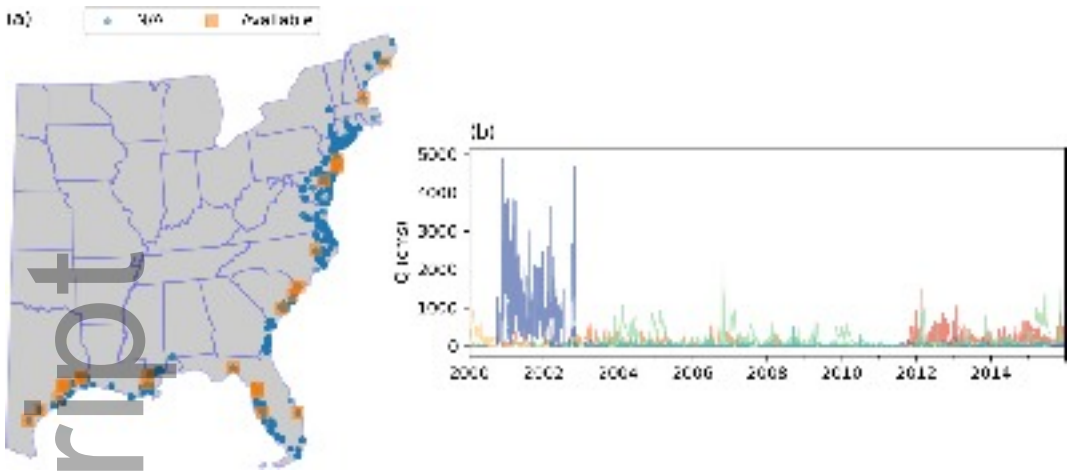

jawr_12983_f3.tiff

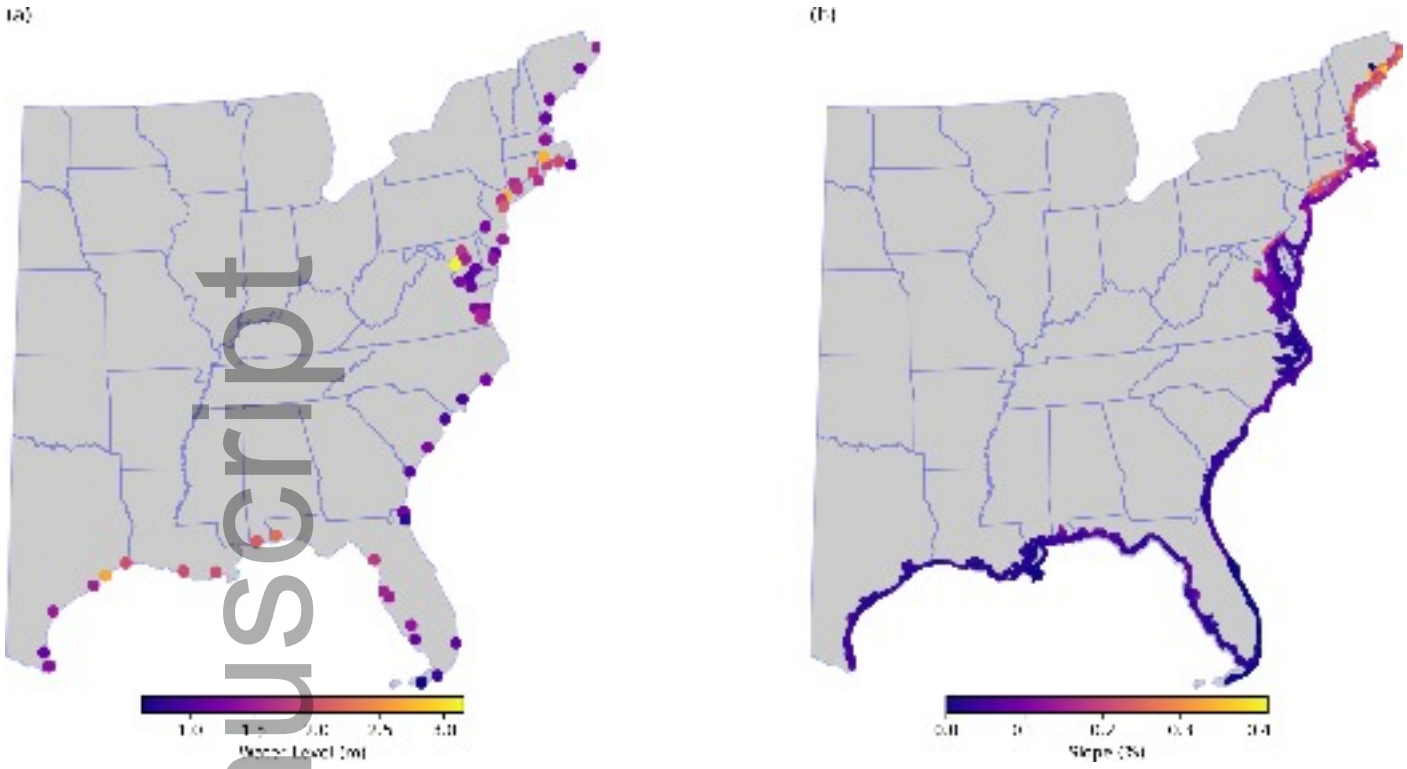

jawr_12983_f4.tiff

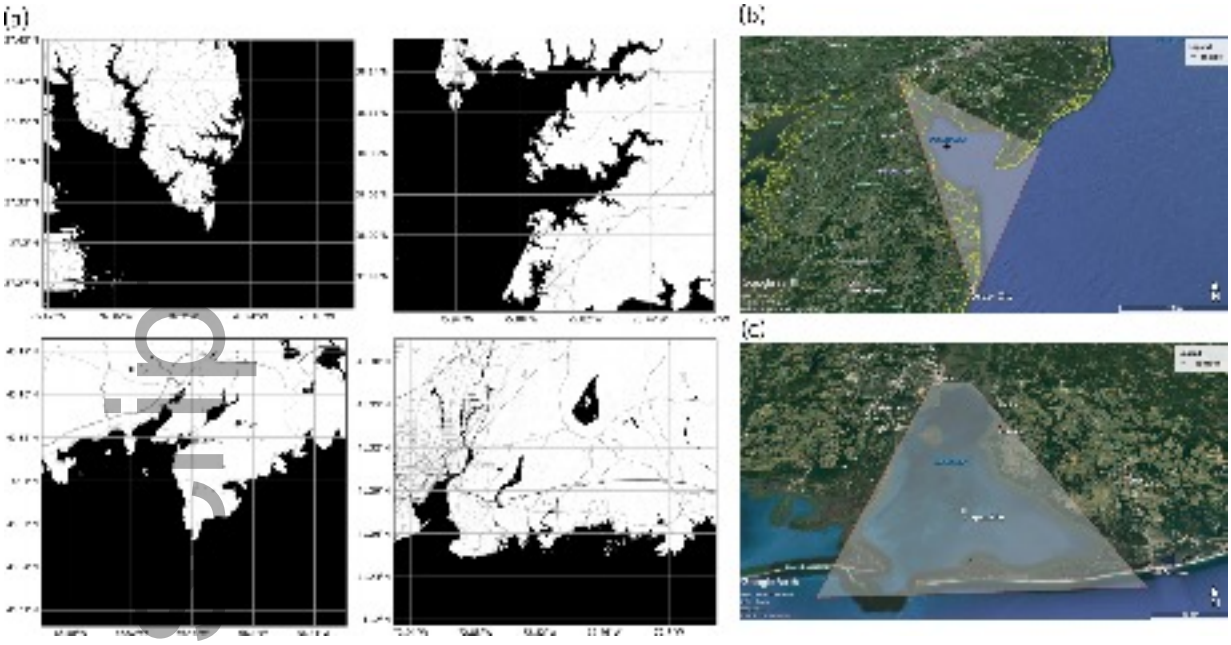

jawr_12983_f5.tiff

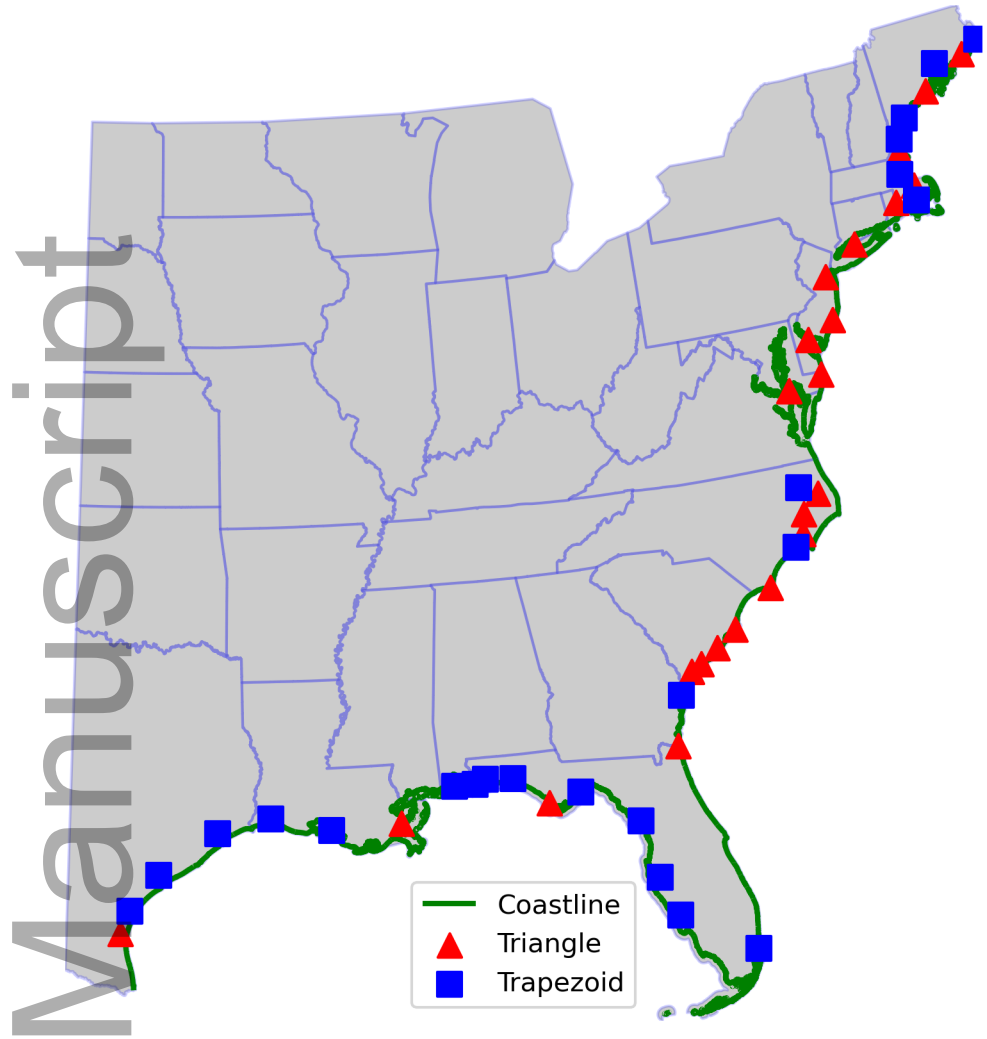

jawr_12983_f6.tiff

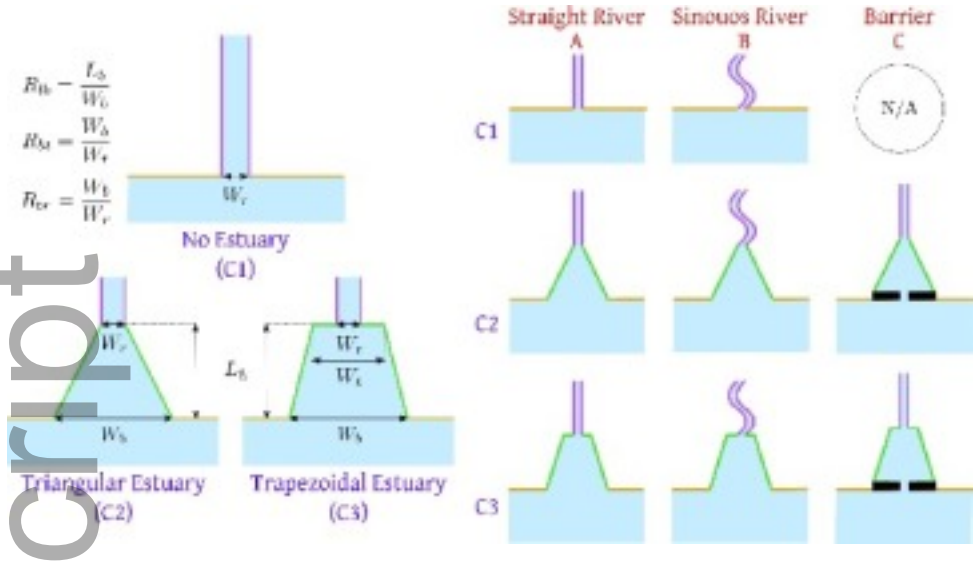

jawr_12983_f7.tiff

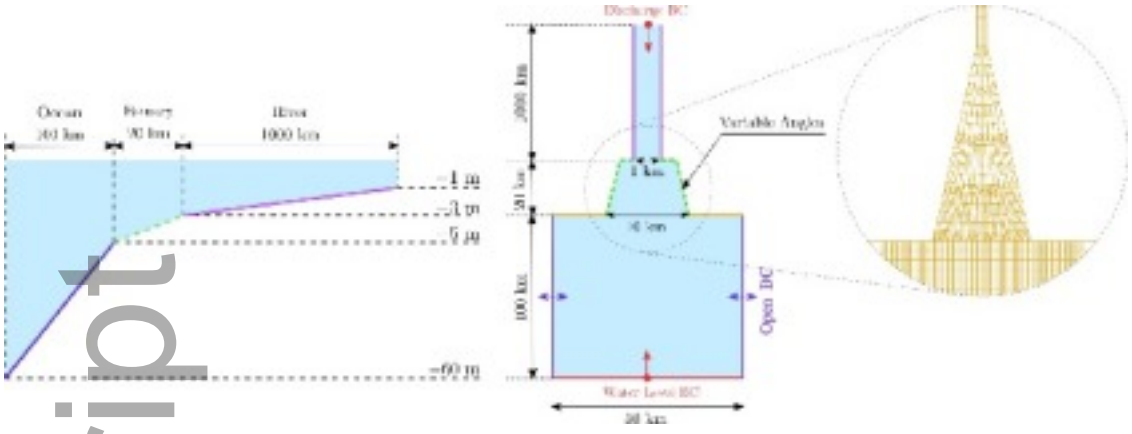

jawr_12983_f8.tiff

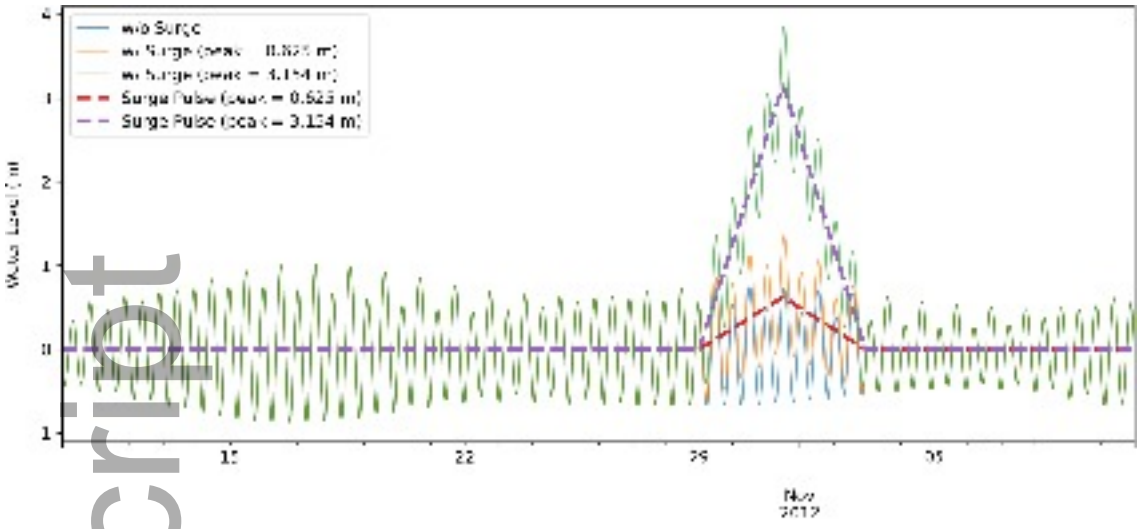

jawr_12983_f9.tiff

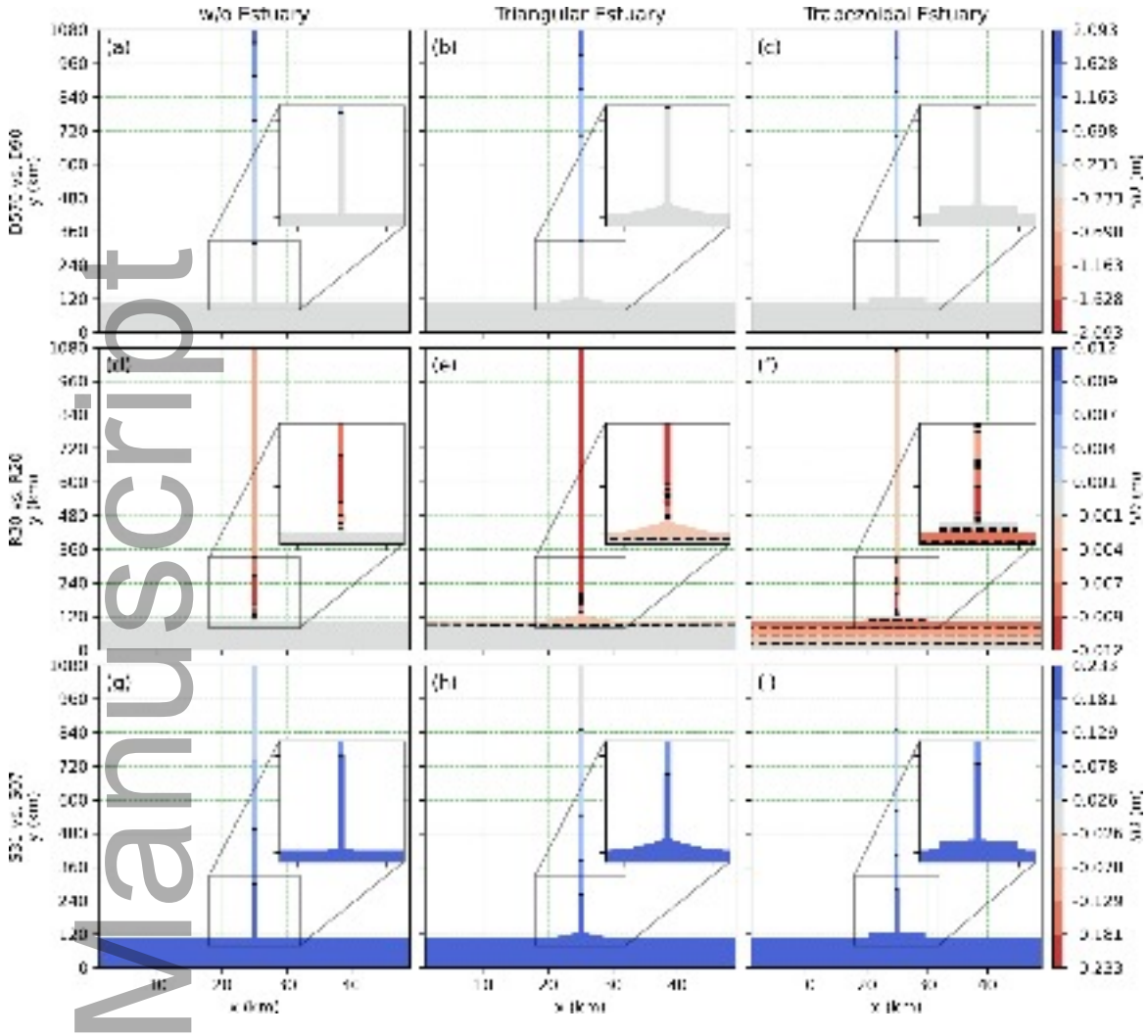

jawr_12983_f10.tiff

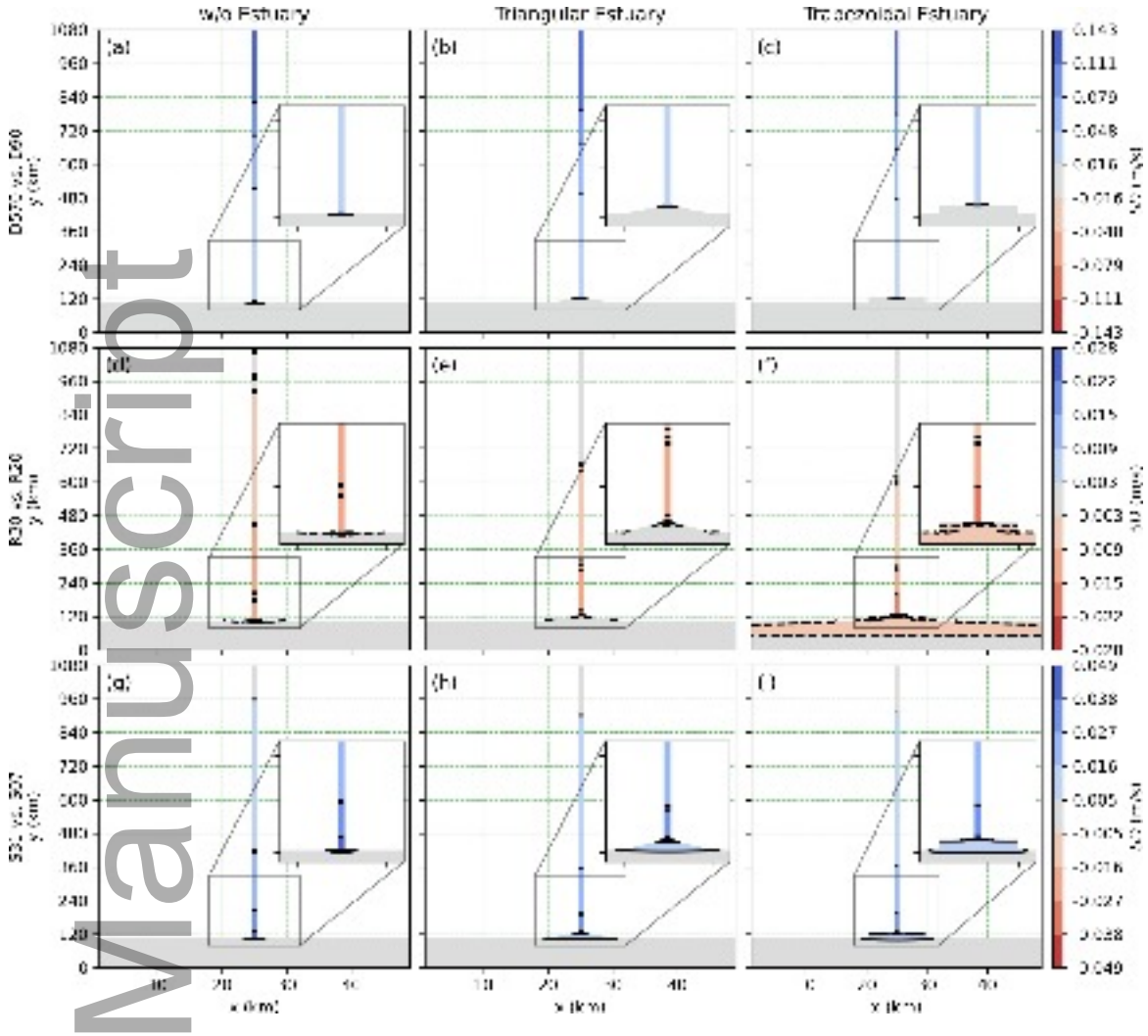

jawr_12983_f11.tiff

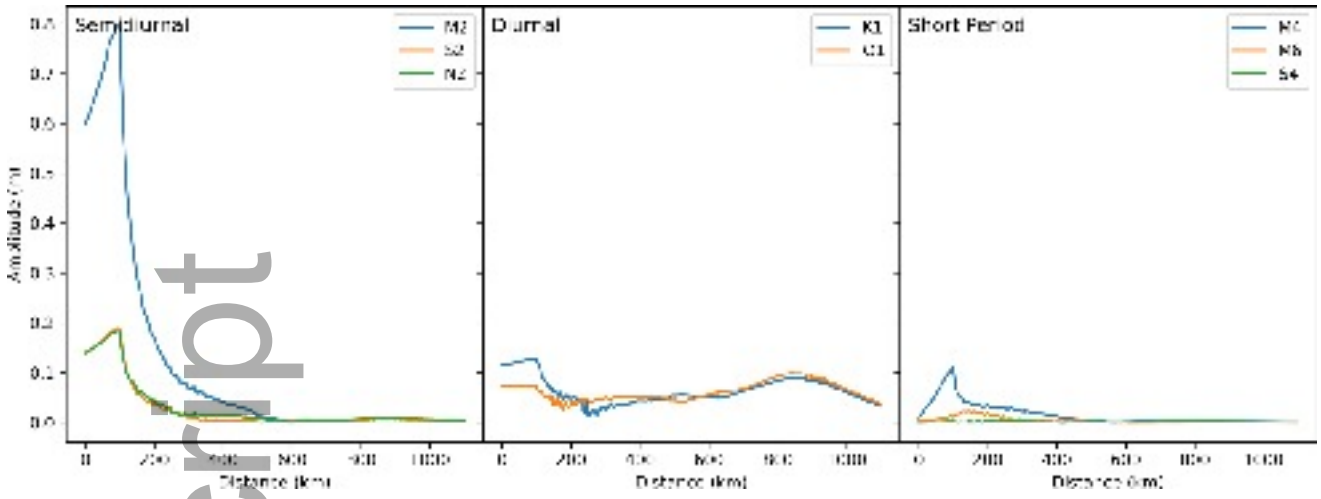

jawr_12983_f12.tiff

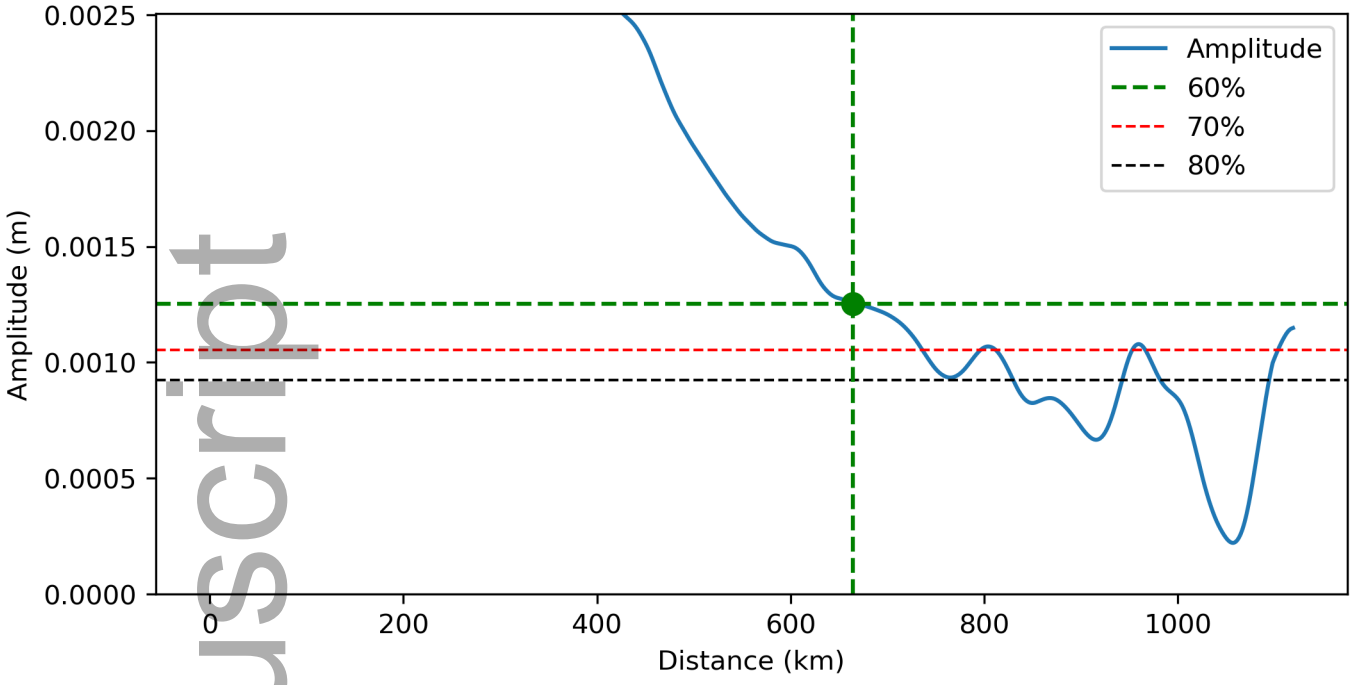

jawr_12983_f13.tiff

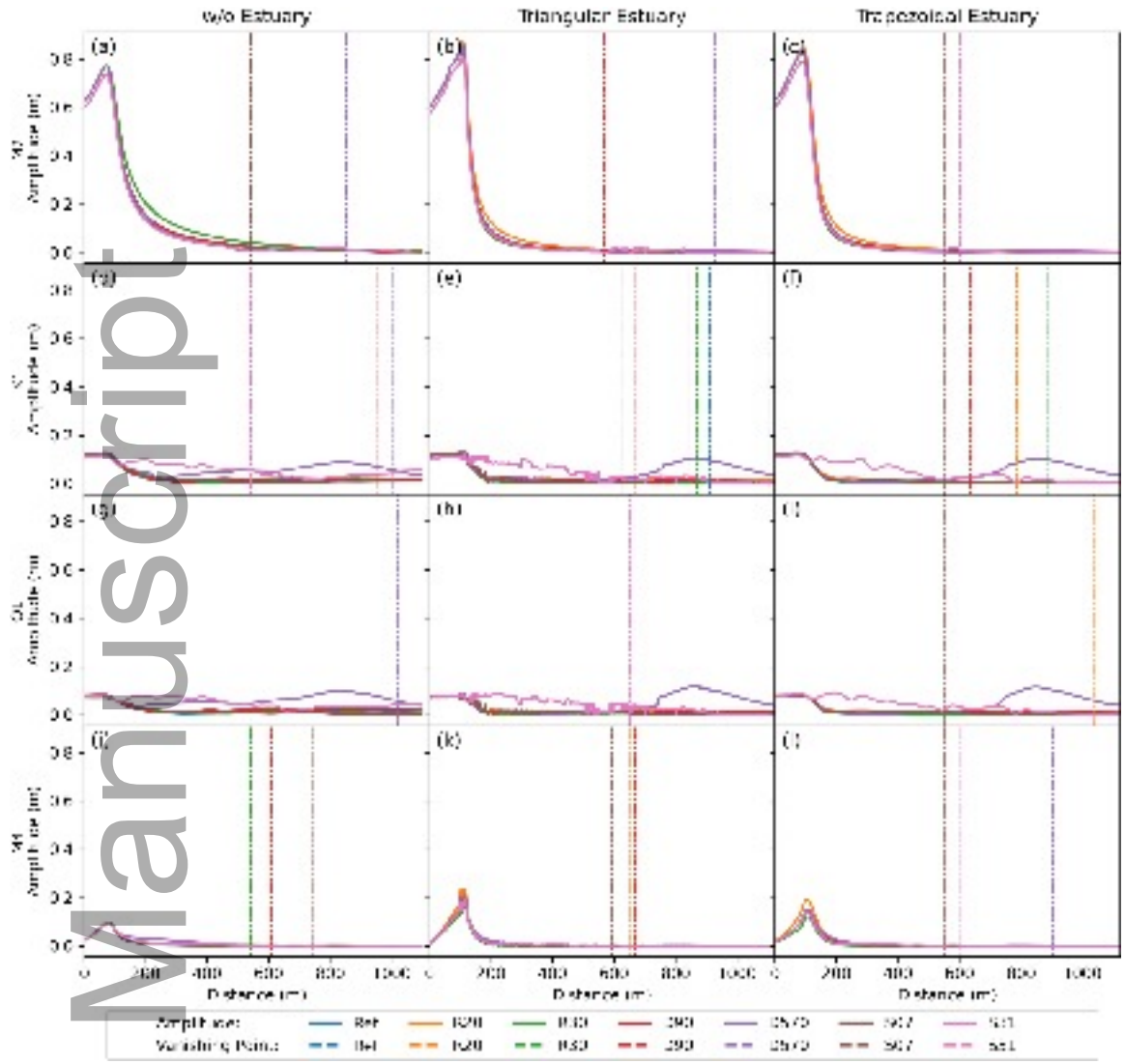

jawr_12983_f14.tiff